SF2A 2016
C. Reylé, J. Richard, L. Cambrésy, M. Deleuil, E. Pécontal, L. Tresse and I. Vauglin (eds)

COULD THE STELLAR MAGNETIC FIELD EXPLAIN THE VERTICAL STRUCTURES IN THE AU MIC DEBRIS DISK?

É. Sezestre[1] and J.-C. Augereau[1]

Abstract.
Recent observations of the edge-on debris disk of AU Mic have revealed asymmetric, fast-moving wave-like structures above its disk midplane. Although asymmetries are frequent in debris disks, no model can readily explain these features. In this paper, we present a model aiming to reproduce such structures, particularly the wave morphology and the high projected speeds. We test the hypothesis of dust emitted by a point source, interacting with the stellar wind and the large-scale magnetic field of the star. We perform numerical simulations of test particle trajectories to explore the available parameter space. The impact of the stellar wind and the magnetic field on the dust dynamics is discussed separately, then together. The stellar wind and, to a smaller extent, the magnetic topology, can reproduce the arches. The observed structures cannot be explained by a single trajectory common to all dust grains emitted intermittently by a fixed point source in space. This excludes a giant collision as the emission process. Therefore, our preferred scenario relies on an orbiting source of dust, possibly a planetary companion, emitting at different epochs.

Keywords: stars: individual: AU Mic, planet-disc interactions, magnetic fields

1 Introduction

AU Mic is an active M-type star in the β Pictoris moving group (23.3 Myr, Mamajek & Bell 2014) with an edge-on debris disk. Recent high contrast imaging with VLT/SPHERE has revealed 5 arch-like structures close to the star (annotated A to E, see fig. 1) in the southeastern side of the disk (Boccaletti et al. 2015). These features have been shown to move away from the star at high speeds, possibly exceeding the local escape velocities. No model can readily explain how to form such fast moving arch-like structures.

In this study, we elaborate on models aiming to explain and reproduce the northwest/southeast asymmetry of the disk, the observed high speeds and the arch-like structures.

We assume that the NW/SE asymmetry can be explained by a local process of dust release, for example emission from a planet or its nearby environment, or because of a dust enhancement due to a giant collision on resonant trapping with a planet. This hypothetic emission source will be called *parent body* in the following, without further specification. The dust is supposed to be exposed to the stellar wind. The resulting wind pressure can put this dust on unbound trajectories, achieving the high projected speeds observed (see sec. 2.1). We explore the interaction between charged dust particles and the stellar magnetic field as a source of vertical elevation for the dust in subsection 2.2. The parametrisation of the model is described in the subsection 2.3. In section 3 we test the influence of the stellar wind (3.1) and the magnetic field (3.2), and then their mutual dependence (3.3).

2 Model

2.1 Stellar wind and radiation pressure

Dust particules are expected to be exposed to a strong stellar wind and to a lesser extent to the radiation pressure, which exerts a net pressure force that can overcome the stellar gravity. The β parameter, the ratio of the pressure to the gravitation forces, quantifies this effect (e.g. Krivov et al. 2006).

[1] Univ. Grenoble Alpes, CNRS, IPAG, F-38000 Grenoble, France

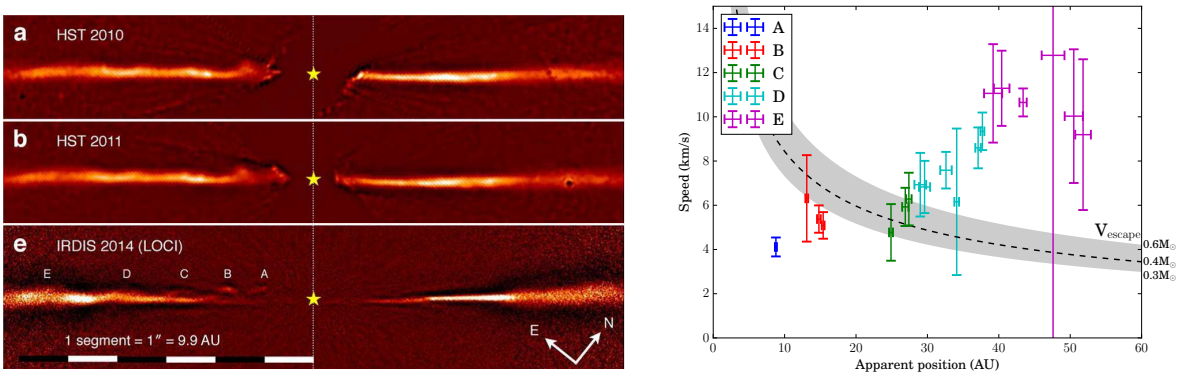

Figure 1. Left: Images of the disk in 2010, 2011 and 2014 extracted from Boccaletti et al. (2015). The five structures are labelled from A to E. **Right:** Apparent velocity of the structures as a function of apparent separation. The grey area corresponds to the projected escape velocity of the system assuming a stellar mass between 0.3 and $0.6 M_{\odot}$.

The trajectory of a grain released from a parent body strongly depends on the β value. Assuming a parent body on a circular orbit, the $0 < \beta < 0.5$ dust particles will remain on bound orbits, with eccentricities increasing with β, while $0.5 < \beta < 1$ particles will be placed on parabolic orbits. Dust particles with $\beta > 1$ will follow unbound, "abnormal" parabolic trajectories. These $\beta > 1$ grains are of particular interest in the context of the AU Mic debris disk because their velocity continuously increases while moving outwards, until it reaches an asymptotic value.

2.2 Magnetic field topology

A 4.2 kG magnetic field has been measured at the stellar surface of AU Mic (Saar 1994). It is supposed to extent at tens of AUs. The interaction *via* the Lorentz force between charged dust particles and a specific magnetic topology can lead to oscillating trajectories around the disk midplane, that may ultimately form arches as observed.

To form an arch, the particle must go upward with respect to the disk midplane, then downward, meaning the net force applied on the grain needs to change sign. These conditions are met if a charged grain evolves in a magnetic field that changes sign on the course of its trajectory.

We suppose that the magnetic axis of the star is misaligned with its rotation axis. We assume that the star has a simple dipole structure but with the field lines emitted from each pole being carried away by the stellar wind. Along the equator, these field lines create a so-called neutral current sheet. At any distance from the star, the neutral current sheet split the disk in two, with one half seeing a magnetic field that has the same strength but an inverse sign compared to the other half of the disk. Due to the misalignment, this current sheet takes the form of a *ballerina skirt* as described in Alfvén (1977). The intersection between the disk midplane and the ballerina skirt is a two-arm spiral as can be seen on figure 2. In the sketch, the brown area corresponds to disk regions located above the current sheet, while the purple area corresponds to regions below the current sheet. In the ideal MHD model, this structure propagates with the stellar wind, as the star rotates. Therefore, the whole structure is in solid rotation with the star, with a period of 4.85 days (Messina et al. 2010).

2.3 Model parameters

In our model, the dust particles are emitted by a parent body on a circular orbit in the disk midplane. They are released with the keplerian speed plus a vertical component. Their charge is constant over the time. The dust grains feel the gravity of the star, the stellar wind pressure, the radiation pressure and the Lorentz force. The 5 key parameters defining the trajectory are (see fig. 2):

- β : the pressure/gravitation forces ratio,
- q/m : the charge/mass ratio,

- R_0 : the radius of the parent body orbit assumed to be circular,
- V_{z0} : the initial vertical speed of the particle,
- θ_0 : the angle between the released point and the intersection of the current sheet with the parent body trajectory.

The trajectories are computed with a 4^{th}-order Runge-Kutta integrator, then rotated and projected to reproduce the images. This leads to an additional free parameter which is the angle α between the observer and the released point.

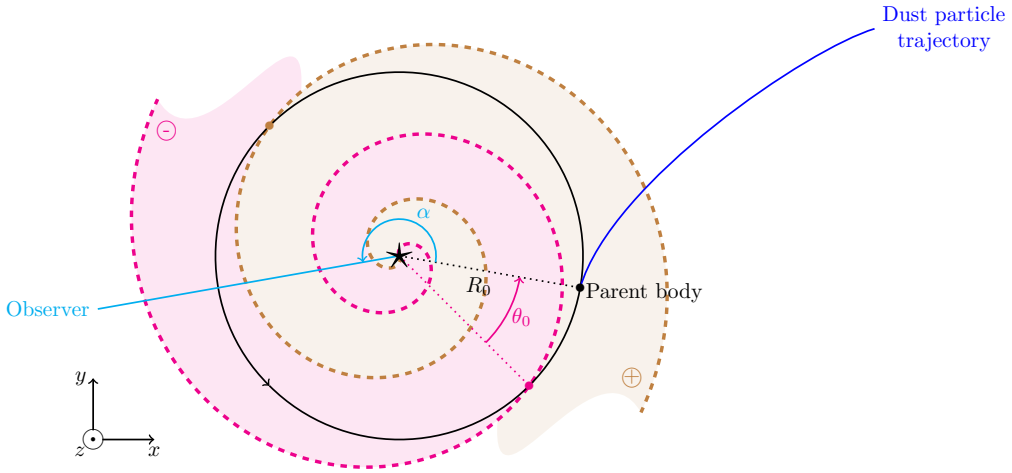

Figure 2. Sketch of the system seen from above. The dashed coloured lines mark the sign change of the magnetic field.

3 Results

3.1 *Ejected dust grains*

In a first step, we ignore the magnetic field and we adjust the observed speeds by projecting the trajectories, considering only α, β and R_0. The movement is thus confined to the disk midplane. We test if a single trajectory can fit all the projected velocities. That supposes a common origin for all the structures, assumed to arise from a static parent body and with self-similar trajectories.

Figure 3 shows the χ^2 map of the speed adjustment. The best fits are obtained for particles emitted at typically 25 AU, with $\beta > 1$ ($\beta \approx 7$). There appears to be a clear dependency between β and R_0.

While the fit is consistent with all the data points, it appears that the A,B structures may require lower R_0 values than the C,D,E structures (for comparison, see fig. 4). That can suggest that either the two groups correspond to two different activity periods for the parent body, or they have a different emission point.

3.2 *Arch formation*

In a second step, we examine the vertical position of the dust particles as a function of time to search for extrema as proxies for arch formation. In this case, the magnetic field is switched on, but any projection effect is neglected. Consequently, we have five parameters characterising the trajectory $(\beta, q/m, R_0, V_{z0}, \theta_0)$. The number of extrema, noted N in the following, corresponds roughly to twice the number of formed arches.

For each parameter, we select 6 values within a broad range and calculate the resulting 7,776 trajectories. A χ^2 value is assigned to each trajectory, which we here define as the sum of the difference between all the extremum elevations and ± 0.5 AU, divided by the number of extrema. This favours a few oscillations around 0.5 AU above and below the disk midplane rather than numerous arches.

As shown in figure 5, different behaviours are possible. The largest number of extrema is achieved for bound particles (e.g. N=77 for $\beta = 0.4$, figure 5). Unbound particles can only form a smaller number of arches. We

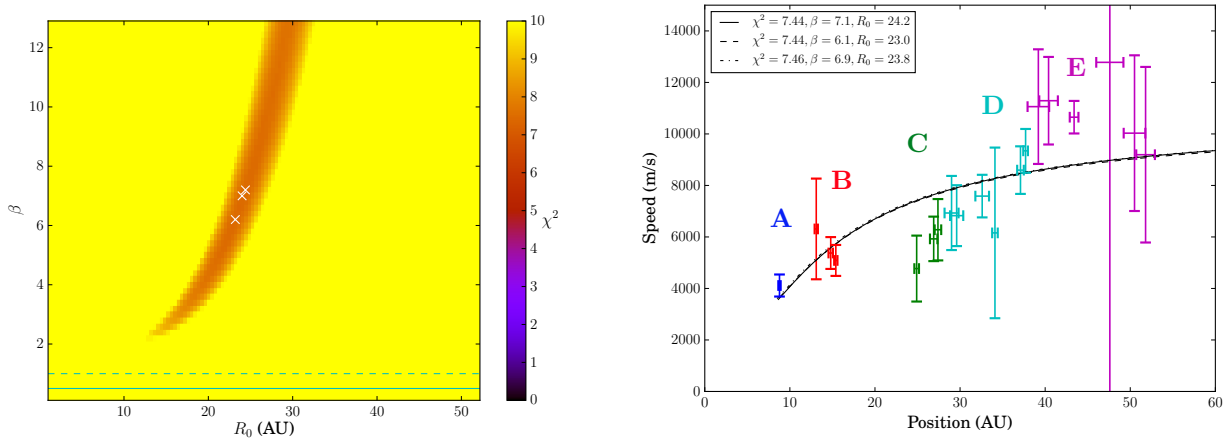

Figure 3. Left: Reduced χ^2 map for the fit of the observed speeds of the 5 structures all together. The light blue line and dashed line correspond respectively to $\beta = 0.5$ and $\beta = 1$. **Right:** Best fits for the speeds, corresponding to the white crosses on left panel.

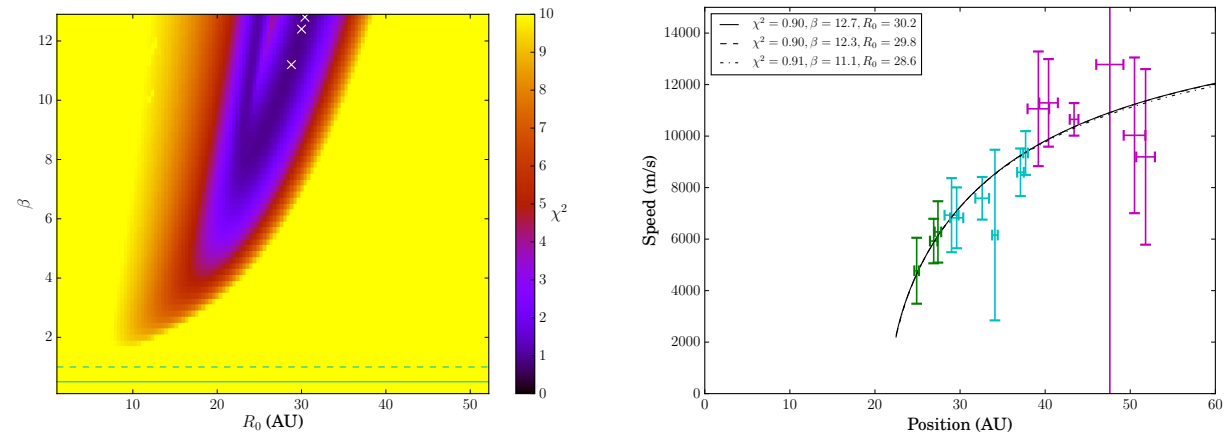

Figure 4. Same as fig. 3, but only for the structures C,D,E.

could not form more than 3 arches with unbound particles, and over 4 extrema, the solutions are only small oscillations around the disk midplane, and no longer elevated arches (see N=8 in figure 5).

The 5-dimension χ^2 array is transformed into probability distributions for each parameter of the model, and presented figure 6. The most probable values are $\beta = 0.4$ and $R_0 = 2$ UA. This test is biased toward inclined, bound orbits. In this case, the code detects one arch every revolution, as the particle move from one side of the disk midplane to the other side during one revolution. As the duration of the simulation is constant and does not depend on R_0, the closest orbits can do more revolution than farthest orbits. Since one arch is detected every revolution, the closer the orbit, the more arches are formed. This is why the bound, closest orbits give the best results in this case.

3.3 Global Adjustment

There is a discrepancy between the results of the two precedent tests. The adjustment of the speeds suggests unbound orbits ($\beta \approx 7$), originating from a parent body far from the star ($R_0 \approx 25$ AU). The formation of arches, on the other hand, favours bound ($\beta < 0.5$), close orbits ($R_0 \approx 10$ AU). This simple model might not be complex enough to reproduce the observations. Nevertheless, that excludes a static source of dust with respect to the observer, ruling out a giant collision process of dust emission.

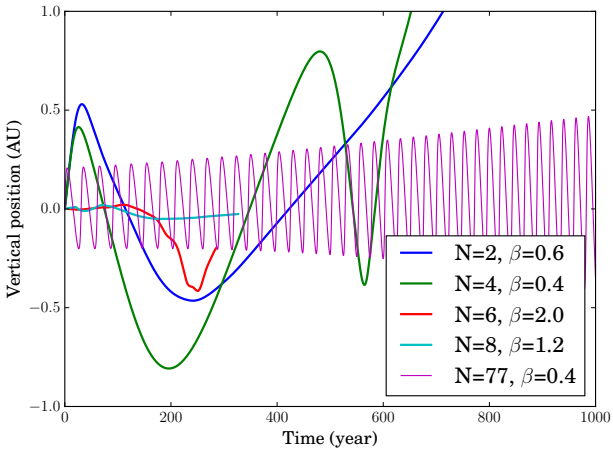

Figure 5. Evolution of vertical elevation over the time for the best trajectories at a given number of extrema N.

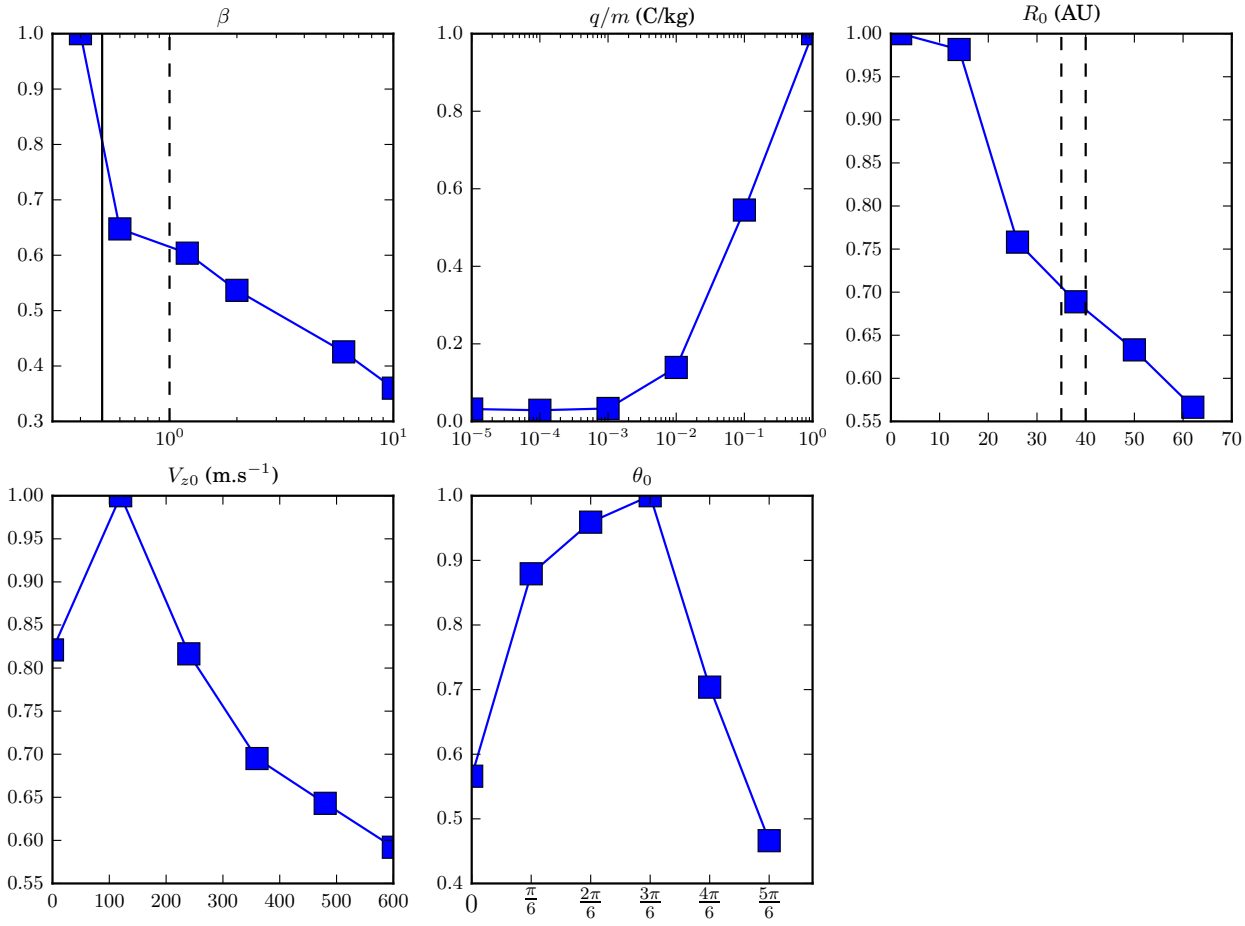

Figure 6. Probability distribution for all the parameters derived from the arch formation. The maximal value is normalised. The dashed vertical lines in the R_0 panel correspond to the position of the planetesimal belt.

We have developed a more complex model to reproduce the arches and their velocities at the same time. Again, we set a few values for each parameters and calculate the trajectories. The χ^2 calculated for each trajectory describes the ability to form each arch separately, with a morphology similar to what is observed, considering the projection effect to account for the different epochs. The trajectory must fit the elevation

above the disk midplane and position of the arch at the observing date, and also go back to the disk midplane consistently with the arch radial extension. Then a non-normalised probability for each parameter is calculated based on the χ^2. The results are presented in figure 7.

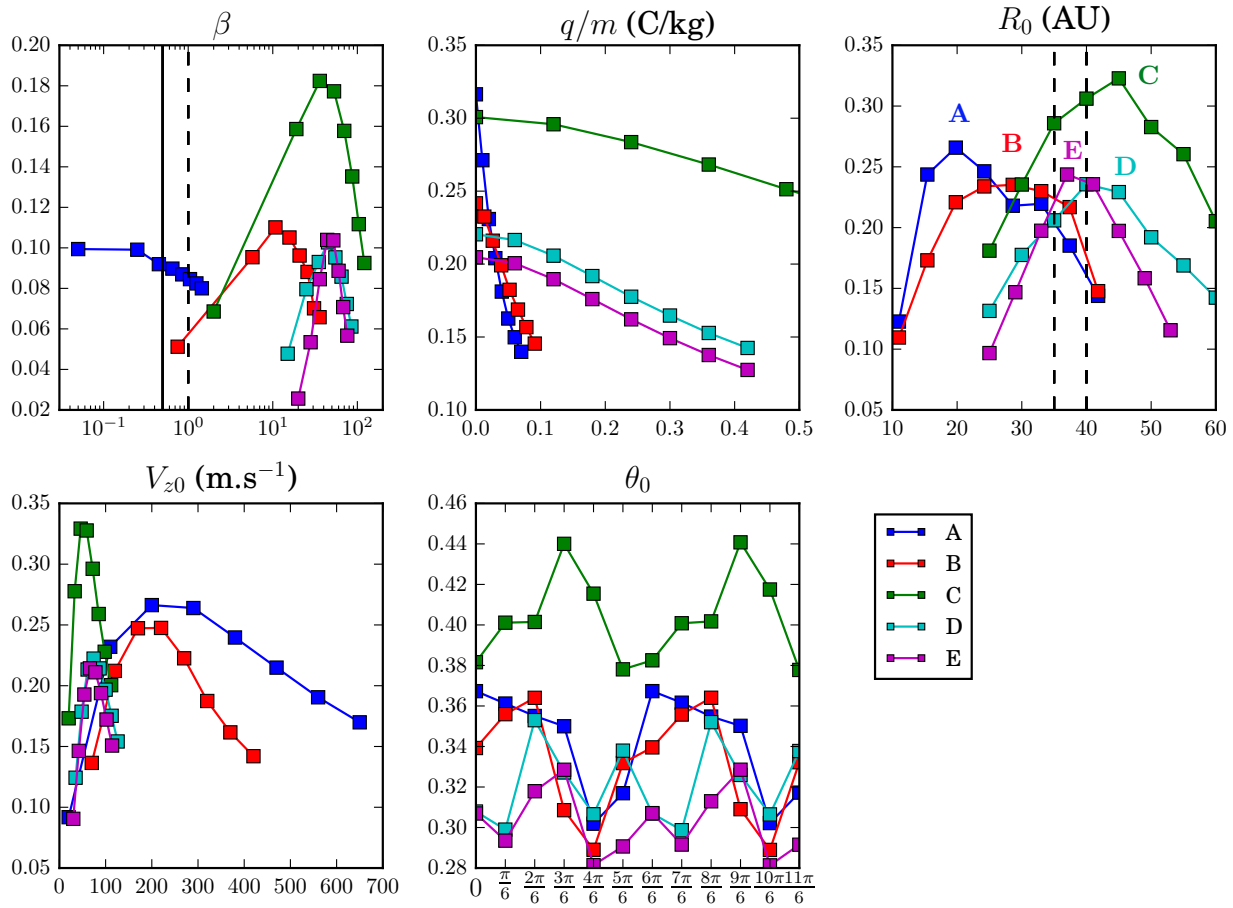

Figure 7. Probability distribution of the parameters, for each structure.

For each structure, we see the most probable value of the five parameters in our model. Again, two groups of structures appear. A,B for one side, with low β, low R_0 ($\approx$ 20 AU) and high V_{z0} values ($\approx$ 200 m.s^{-1}). They are the closest structures, the most elevated, and are moving slower than the others. On the other side, the C,D,E structures have higher β ($\approx$ 30), higher R_0 ($\approx$ 40 AU) and lower V_{z0} values ($\approx$ 50 m.s^{-1}). These structures seem consistent with a parent body included inside the planetesimal belt, estimated to be at 35-40 AU from the star (Augereau & Beust 2006; Strubbe & Chiang 2006; Schüppler et al. 2015). For all the structures, the charge is very small, meaning that the magnetic field is maybe not the most important component of our model to reproduce the structures, compared to the initial vertical speed. We see also a symmetric behaviour on both sides of the disk for θ_0.

4 Conclusion

From the models developed here, we can point out some behaviours for the dust particles:

- We need unbound dust particles to explain the projected speeds: the structures are evolving fast.
- A ballerina skirt magnetic field topology can produce oscillating trajectories, but not 5 arches.
- Several arches formation by a single grain and high velocities seem to require inconsistent β values.

- A more complex model seems to argue for two different parent body for the structures, always farthest than 20 AU from the star.

We can set appart the hypothesis of a single point of emission static with respect to the observer, like in the case of a giant collision. A parent body inside the planetesimal belt releasing periodically dust is favoured by the models.

References

Alfvén, H. 1977, Rev. Geophys., 15, 271
Augereau, J.-C. & Beust, H. 2006, A&A, 455, 987
Boccaletti, A., Thalmann, C., Lagrange, A.-M., et al. 2015, Nature, 526, 230
Krivov, A. V., Löhne, T., & Sremčević, M. 2006, A&A, 455, 509
Mamajek, E. E. & Bell, C. P. M. 2014, Mon. Not. R. Astron. Soc., 445, 2169
Messina, S., Desidera, S., Turatto, M., Lanzafame, A. C., & Guinan, E. F. 2010, Astron. & Astrophys., 520, A15
Saar, S. H. 1994, in Infrared Sol. Phys. Proc. 154th Symp. Int. Astron. Union No. 1, 1–5
Schüppler, C., Löhne, T., Krivov, a. V., et al. 2015, Astron. Astrophys., 97, 1
Strubbe, L. E. & Chiang, E. I. 2006, Astrophys. J., 648, 652